Performance Analysis of a Direct Torque Controlled PV Water Pumping System Using Grey Wolf Optimizer and Incremental Conductance Maximum Power Point Tracking under Variable Irradiance

Oussama Idbouhouch
Laboratory of Digital Engineering for Leading Technologies and Automation (DELTA), National Higher School of Arts and Crafts (ENSAM), Hassan II University, Casablanca, Morocco | Green Energy Park Research Platform (GEP), Research Institute for Solar Energy and New Energies (IRESEN), Mohammed VI Polytechnic University (UM6P), Benguerir, Morocco
oussam.idbouhouch-etu@etu.univh2c.ma (corresponding author)

Mourad Zegrari
Laboratory of Digital Engineering for Leading Technologies and Automation (DELTA), National Higher School of Arts and Crafts (ENSAM), Hassan II University, Casablanca, Morocco
zegrari.ensam@gmail.com

Nabila Rabbah
Laboratory of Cyber Physical Systems (LCCPS), National Higher School of Arts and Crafts (ENSAM), Hassan II University, Casablanca, Morocco
nabila_rabbah@yahoo.fr

Received: 23 November 2025 | Revised: 15 December 2025, 26 December 2025, 31 December 2025, and 8 January 2026 | Accepted: 9 January 2026

Licensed under a CC-BY 4.0 license | Copyright (c) by the authors | *DOI: https://doi.org/10.48084/etasr.16460*

ABSTRACT

This paper presents a performance analysis of a Photovoltaic (PV) water pumping system driven by an Induction Motor (IM) and controlled through the Direct Torque Control (DTC) strategy. The DTC approach was implemented to directly regulate the electromagnetic torque and stator flux, thereby ensuring fast dynamic response and high-efficiency operation. To optimize the energy conversion process under variable irradiance, two Maximum Power Point Tracking (MPPT) techniques were integrated into the DC–DC boost converter: the Incremental Conductance (INC) and the Grey Wolf Optimizer (GWO). The main objective of this study is to assess and compare the dynamic and steady-state performance of the DTC–INC and DTC–GWO configurations under both uniform and partially shaded conditions. The simulation results, performed using MATLAB/Simulink, show that while both strategies achieve stable operation under normal irradiance, the GWO-based MPPT exhibits superior adaptability under partial shading by accurately locating the Global Maximum Power Point. This results in an approximate 32% increase in hydraulic power relative to the INC approach, thereby improving torque stability, accelerating convergence, and increasing hydraulic efficiency. This study contributes to the advancement of intelligent PV-based pumping systems by integrating heuristic optimization and high-performance motor control, offering a promising solution for sustainable water supply in remote and semi-arid regions.

Keywords-photovoltaic water pumping; direct torque control; grey wolf optimizer; incremental conductance; MPPT; partial shading; induction motor

I. INTRODUCTION

Transition toward renewable energy systems has become a global imperative, particularly in the context of sustainable water management in rural and semi-arid regions. PV water pumping systems represent one of the most promising alternatives to conventional diesel-driven pumps, offering environmentally friendly, cost-effective, and maintenance-free solutions for irrigation and drinking water supply. The continuous decrease in PV module costs and improvements in power electronics have accelerated the deployment of such systems, contributing significantly to decentralized clean energy generation [1]. In isolated and agricultural regions, Solar Water Pumping (SWP) represents a solution to address energy, water, and socio-economic challenges. In the absence of reliable electrical infrastructure, PV systems provide decentralized and autonomous access to water for domestic use, irrigation, and livestock farming [2]. In parallel with technological progress, SWP systems have seen a rapid expansion. According to the Global Off-Grid Lighting Association (GOGLA), approximately 291,269 solar water pumps were sold globally in 2024, a significant increase compared to previous years [3]. Within Sub-Saharan Africa, CLASP's Spotlight on Solar Water Pumps examines irrigation gaps across 11 countries and shows that, despite very low adoption due to high upfront costs, solar pumps offer major economic and climate benefits. It was estimated that closing these gaps with solar pumping could avoid about 410 Mt of CO_2 annually, significantly improve food security for tens of millions of people, raise agricultural yields, reduce labor burdens, and generate large fuel-cost savings compared to diesel systems [4]. On a global scale, the International Renewable Energy Agency (IRENA) emphasizes the growing contribution of off-grid renewable systems, particularly for productive uses such as water pumping [1]. This adoption reinforces the importance of advancing MPPT algorithms, motor control strategies, and integrated PV system design to further enhance the performance and reliability of SWP systems. Research also examined the long-term degradation and reliability of PV inverters operating under semi-arid conditions, revealing efficiency declines of up to 3–4% over five years and underscoring the necessity for predictive maintenance strategies in harsh climates [5].

Despite their advantages, PV water pumping systems suffer from inherent intermittency of solar irradiance and nonlinear PV characteristics, which lead to power fluctuations and reduced system efficiency. The implementation of MPPT algorithms in conjunction with DC–DC converters is therefore significant to ensure optimal energy extraction from the PV generator. Traditional MPPT methods, such as Perturb and Observe (P&O) and INC, have been employed due to their simplicity and ease of implementation [6]. Authors in [7] demonstrated how combining a fast dynamic control strategy on the motor side with hybrid MPPT algorithms significantly improves system tracking accuracy, response under rapidly changing irradiance, and overall hydraulic output. The findings highlighted the importance of coordinated control between the PV generator, the power converter stages, and the IM drive. However, these techniques exhibit limited performance under partial shading and rapid irradiance variations, where multiple local maxima appear in the power voltage curve, often causing the system to settle at suboptimal points [8, 9]. To overcome these limitations, the integration of bio-inspired metaheuristic algorithms, such as Particle Swarm Optimization (PSO) [10], Ant Colony Optimization (ACO) [11], and GWO [12, 13], has been explored. These methods emulate intelligent search mechanisms found in nature, enabling global MPPT under complex environmental conditions. Among them, the GWO algorithm has attracted particular attention for its fast convergence, robust adaptability, and simple parameter tuning, making it well-suited for embedded MPPT applications in PV systems. Moreover, the integration of GWO-based MPPT with various inverter control techniques, such as SPWM, THIPWM, and SVPWM, has been comparatively evaluated, demonstrating that SVPWM achieves superior voltage quality under uniform irradiance, while THIPWM remains more resilient under partial shading [14]. In the same context, authors in [15] studied a single-stage PV water-pumping system that connects a PV array directly to multilevel inverter driving an IM pump through V/f control. They focused on reducing the number of switches compared to a conventional H-bridge inverter and improving voltage waveform quality using SPWM modulation. Through PSIM simulation under a variable daily climate profile, the results showed that the proposed topology delivers smoother voltage waveforms with lower harmonic distortion, ensures stable motor operation throughout the day, and achieves better pumping performance compared to the traditional inverter configuration. On the other hand, efficient energy conversion from the electrical to the mechanical domain requires robust motor control techniques. Conventional vector control and Field-Oriented Control (FOC) schemes, though effective, rely on complex transformations and parameter estimations that increase computational burden and implementation cost [16]. In contrast, the DTC method [17, 18], offers fast dynamic response, simplified structure, and direct regulation of electromagnetic torque and stator flux, making it highly attractive for PV-driven IM applications. The DTC technique provides high performance without requiring current regulators or coordinate transformations, thereby improving response speed and reducing system complexity.

DTC-based drives for renewable energy applications, particularly in PV systems, have been investigated [19, 20]. However, most research has analyzed the integration of DTC with advanced MPPT algorithms, such as PSO or fuzzy logic only under uniform irradiance conditions, typically corresponding to Standard Test Conditions (STC). Attention has also been directed toward fault-tolerant inverter design and control reliability, where embedded implementations of three-phase SVPWM inverters using SiC MOSFETs have shown the ability to detect and mitigate phase imbalance faults across multiple testing layers (MIL, SIL, PIL), improving resilience under component degradation [21]. Under these stable scenarios, the system performance is evaluated assuming constant solar input, which does not fully represent the dynamic behavior encountered in real-world PV installations. Consequently, the combined impact of intelligent MPPT control and DTC torque-flux regulation on system efficiency, especially under variable or partially shaded conditions, remains insufficiently explored.

TABLE I. LIST OF ABBREVIATIONS

Abbreviations	Nomenclature
ACO	Ant Colony Optimization
DC–AC	Alternating Current
DC	Direct Current
DTC	Direct Torque Control
FOC	Field-Oriented Control
GMPP	Global Maximum Power Point
GWO	Grey Wolf Optimizer
H	Head (manometric)
HC	Hysteresis Controller
IGBT	Insulated-Gate Bipolar Transistor
INC	Incremental Conductance
LMPP	Local Maximum Power Point
MPPT	Maximum Power Point Tracking
MIL	Model-in-the-Loop
P&O	Perturb and Observe
PSC	Partial Shading Conditions
PIL	Processor-in-the-Loop
PSO	Particle Swarm Optimization
PV	Photovoltaic
IM	Induction Motor
SIL	Software-in-the-Loop
STC	Standard Test Conditions
SWP	Solar Water Pumping

In particular, DTC-based PV pumping systems are commonly evaluated under uniform irradiance conditions, where the PV power-voltage characteristic exhibits a single maximum. Under such assumptions, the dynamic interaction between the MPPT algorithm and the motor drive is not fully revealed. However, real-world PV pumping installations frequently operate under Partial Shading Conditions (PSC), where multiple local maxima arise, and where the coupling between source-side power optimization and motor-side torque control becomes critical. Existing works rarely investigate how heuristic global MPPT algorithms interact with fast torque-flux control strategies such as DTC, nor do they quantify the resulting impact on hydraulic performance. This limitation motivates the need for a system-level investigation that goes beyond electrical power tracking and evaluates the full electromechanical-hydraulic behavior of PV-driven pumping systems under realistic operating conditions. Addressing this limitation is essential to assess the adaptability, convergence speed, and hydraulic stability of DTC-controlled PV pumping systems operating in realistic solar environments.

This study proposes and systematically evaluates a DTC-controlled PV water pumping system integrating both a classical INC MPPT and a metaheuristic GWO MPPT. While DTC, INC, and GWO have each been individually reported in the literature, their coordinated integration and comparative assessment within a DTC-driven IM pumping system under PSC have not been sufficiently investigated. The proposed configuration combines the fast torque-flux dynamic regulation of DTC with the global search capability of the GWO algorithm, enabling effective interaction between motor-side electromechanical control and source-side power optimization. Unlike most existing DTC-based PV pumping studies, which are limited to uniform irradiance operation, this work explicitly analyzes dynamic and partially shaded conditions that generate multiple local maxima, thereby reflecting realistic field operation.

TABLE II. LIST OF VARIABLES

Variables	Nomenclature
V_{pv}	Output voltage of the PV generator
D	Duty cycle of the DC-DC converter
V_{dc}	DC bus voltage
V_a, V_b, V_c	Stator phase voltages
S_a, S_b, S_c	Switching functions (0 or 1) for inverter control
$V_{s\alpha}, V_{s\beta}$	Stator voltages along the α–β axes
$i_{s\alpha}, i_{s\beta}, i_{r\alpha}, i_{r\beta}$	Stator and rotor currents along the α–β axes
$\Phi_{s\alpha}, \Phi_{s\beta}, \Phi_{r\alpha}, \Phi_{r\beta}$	Stator and rotor flux along the α–β axes
T_e	Electromagnetic torque
T_r	Load torque
$R_{s\alpha}$, $R_{s\beta}$	Stator resistances along the α–β axes
R_r	Rotor resistance
L_s, L_r	Stator and rotor inductances
M	Mutual inductance
P	Number of pole pairs of the machine
H	Total manometric head
Q	Flow rate of the pump
H_g	Geodetic head
K_c	Proportionality constant
Ω	Angular speed of the motor
Ψ	Coefficient depending on pipe diameter and frictional losses
V_{mpp}	Voltage at maximum power point
I_{mpp}	Current at maximum power point
V_{oc}	Open-circuit voltage
I_{sc}	Short-circuit current
I_{pv}	Output current of the PV generator
P_{pv}	Instantaneous power of the PV generator
η	Efficiency

Furthermore, the contribution of this study extends beyond electrical performance by quantifying the impact of MPPT strategy on electromagnetic torque stability, motor speed, flow rate, and delivered hydraulic power. Through this comprehensive electromechanical-hydraulic evaluation, the paper establishes a practical and application-oriented framework for the design of robust PV water pumping systems.

II. CHARACTERISTICS OF THE PV PUMPING SYSTEM

A. System Description and Modeling

Water pumping is one of the most significant PV applications, particularly for meeting water needs in remote areas. Moreover, it helps to mitigate the negative environmental impact associated with diesel-based pumping installations. The implementation of a PV water pumping system for agricultural irrigation in Isfahan, Iran, resulted in an estimated annual reduction of 4.8 tons of CO_2 emissions, compared to an equivalent grid-based pumping configuration [22]. The IM, although not widely addressed in existing research, represents a cost-effective and readily available solution, offering operation and control simplicity. In the context of irrigation and water pumping, maintaining proper flow regulation is crucial. Advanced control techniques applied to IMs facilitate this regulation and ensure enhanced system performance [23]. The overall structure of a PV water pumping system is depicted in Figure 1.

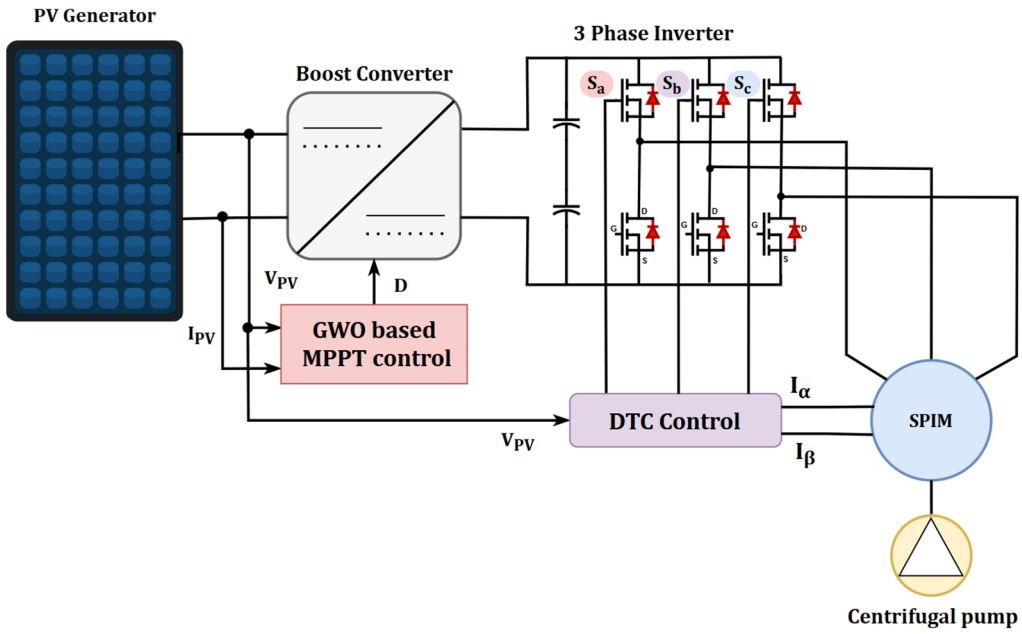

Fig. 1. General architecture of the PV water pumping application.

A DC-DC boost converter is utilized to perform MPPT while increasing the DC voltage generated by the PV module. The Duty cycle (D) of the converter switch is determined through an MPPT controller that integrates the INC method with the GWO. The DC/AC conversion stage comprises a three-phase inverter operating through eight distinct switching states, implemented using the Insulated-Gate Bipolar Transistors (IGBT) switches to regulate both the magnitude and frequency of the stator voltages (Figure 2). The vector representation of each IGBT switching state is illustrated in Figure 3.

$$v = \frac{2}{3} \cdot V_{dc} \left(S_a + S_b e^{j\frac{2\pi}{3}} + S_c e^{j\frac{4\pi}{3}} \right) \quad (5)$$

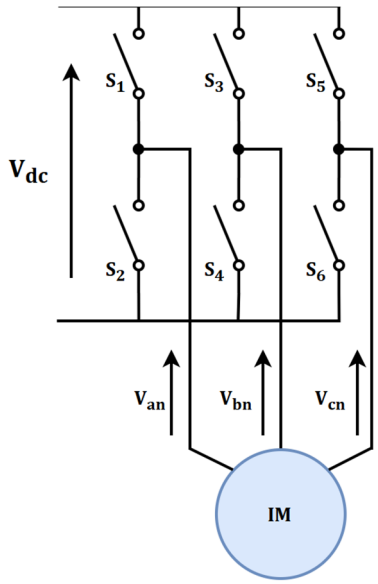

Fig. 2. Three-phase inverter configuration supplying the three-phase IM.

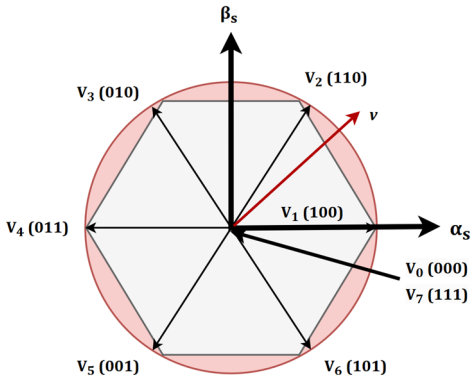

Fig. 3. Operating conditions of a three-phase inverter: vector representation of voltages.

According to [24, 25], the stator phase voltages are defined in (1), where V(a,b,c) represent the three stator phase voltages, Vdc corresponds to the DC bus voltage, and S(a,b,c) are the switching functions, each taking binary values of 0 or 1. The output voltage of the inverter is expressed in (2) and (3) through a vector representation approach. The resulting three-phase voltage system is established in (4), and the variable v can then be expressed as indicated in (5). This formulation enables the calculation of the voltage vector associated with each sector in the space-vector representation:

$$\begin{bmatrix} V_{an} \\ V_{bn} \\ V_{cn} \end{bmatrix} = \frac{V_{dc}}{3} \cdot \begin{bmatrix} 2 & -1 & -1 \\ -1 & 2 & -1 \\ -1 & -1 & 2 \end{bmatrix} \cdot \begin{bmatrix} S_a \\ S_b \\ S_c \end{bmatrix} \quad (1)$$

$$\vec{v} = v_\alpha + jv_\beta \quad (2)$$

$$\begin{bmatrix} V_\alpha \\ V_\beta \end{bmatrix} = \frac{2}{3} \cdot \begin{bmatrix} 1 & -\frac{1}{2} & -\frac{1}{2} \\ 0 & \frac{\sqrt{3}}{2} & -\frac{\sqrt{3}}{2} \end{bmatrix} \cdot \begin{bmatrix} V_{an} \\ V_{bn} \\ V_{cn} \end{bmatrix} \quad (3)$$

$$\begin{bmatrix} V_{an} \\ V_{bn} \\ V_{cn} \end{bmatrix} = V_m . \begin{bmatrix} \cos(\omega t + \varphi) \\ \cos(\omega t + \varphi - \frac{2\pi}{3}) \\ \cos(\omega t + \varphi - \frac{4\pi}{3}) \end{bmatrix} \quad (4)$$

B. Characterization and Modeling of the IM

The IM was chosen for this application because of its low cost, robust design, and high operational reliability. Structurally, unlike single-phase IMs, which rely on a main and an auxiliary winding with a capacitor to create a phase shift, the three-phase IM naturally produces a rotating magnetic field through its three stator windings displaced by 120° electrically [23]. The DC-AC conversion stage employs IGBTs to control the three-phase motor. Due to its nonlinear and asymmetric nature, the IM presents modeling challenges, primarily arising from differences in stator resistance values. The stator and rotor voltage relationships, typically expressed in a stationary reference frame, are formulated based on established models [26]. The mathematical expressions for the stator flux and the electromagnetic torque are defined in (8) and (9), respectively. Table III shows the parameters of the IM.

$$\begin{cases} V_{s\alpha} = R_{s\alpha} i_{s\alpha} + \frac{d\Phi_{s\alpha}}{dt} \\ V_{s\beta} = R_{s\beta} i_{s\beta} + \frac{d\Phi_{s\beta}}{dt} \end{cases} \quad (6)$$

$$\begin{cases} 0 = R_r i_{r\alpha} + \frac{d\Phi_{r\alpha}}{dt} + \omega\Phi_{r\beta} \\ 0 = R_r i_{r\beta} + \frac{d\Phi_{r\beta}}{dt} + \omega\Phi_{r\alpha} \end{cases} \quad (7)$$

$$\begin{cases} \Phi_{s\alpha} = L_s i_{s\alpha} + M i_{r\alpha} \\ \Phi_{s\beta} = L_r i_{s\beta} + M i_{r\beta} \end{cases} \quad (8)$$

$$T_e = \frac{3 \cdot P}{2} \left[\Phi_{s\alpha} \cdot i_{s\beta} - \Phi_{s\beta} \cdot i_{s\alpha} \right] \quad (9)$$

where $V_{s\alpha}, V_{s\beta}$ are the stator voltages along the α–β axes, $i_{s\alpha}, i_{s\beta}, i_{r\alpha}, i_{r\beta}$ are the stator and rotor currents along the α–β axes, $\Phi_{s\alpha}, \Phi_{s\beta}, \Phi_{r\alpha}, \Phi_{r\beta}$ are the stator and rotor flux along the α–β axes, T_e is the electromagnetic torque, $R_{s\alpha}$, $R_{s\beta}, R_r$ are the stator resistances along the α–β axes and rotor resistance, L_s, L_r are the stator and rotor inductances, M is the Mutual inductance, and P is the number of pole pairs of the machine.

TABLE III. IM PARAMETERS

IM Parameters	Values
Nominal power (P) [kW]	1.5
Rated speed(Ω) [rpm]	1420
Nominal frequency (f) [Hz]	50
Stator resistance (Rs) [Ω]	4.850
Rotor resistance (Rr) [Ω]	3.805
Stator inductance (Ls) [H]	0.274
Rotor inductance (Lr) [H]	0.274
Mutual inductance (M) [H]	0.258
Number of pole pairs (P)	2
Rated voltage [V]	230

C. Modeling of the Centrifugal Pump

In the field of water pumping, two main categories of hydraulic machines can be distinguished. The first group consists of positive displacement pumps, which move a fixed volume of fluid per cycle (such as piston, diaphragm, or gear pumps). These devices can deliver high pressures at low flow rates but are generally more complex and expensive to manufacture. The second group includes rotodynamic pumps, which transfer kinetic energy to the fluid through a rotating impeller, among which centrifugal pumps are the most common. These pumps are widely employed for their simplicity, robustness, low cost, and ability to handle large flow rates.

In the specific context of PV solar pumping, where the available power fluctuates with solar irradiance and the motor speed is adjusted by the inverter, the centrifugal pump emerges as the most suitable option. This is because its load torque follows a quadratic relationship with the rotational speed, as expressed in (10), which aligns naturally with the variations in power generated by the PV array [27]. Furthermore, it easily accommodates variable-speed operation and remains an economical solution for applications such as irrigation and potable water supply.

The relationship between the head (H) and the flow rate (Q) within the pipeline network is given by (11), where H is the total manometric head, Q is the flow rate, Hg is the geodetic head, and Ψ is a coefficient dependent on the pipe diameter and the cumulative frictional losses throughout the network.

$$T_r = k_c \Omega^2 \quad (10)$$

where k_c is a proportionality constant.

$$H = H_g + \Psi Q^2 \quad (11)$$

III. CONTROL STRATEGY AND METHOD

A. GWO-Based MPPT

The GWO algorithm is a metaheuristic optimization approach inspired by the cooperative behavior and hierarchical structure of grey wolves. The leadership hierarchy is composed of the alpha (α), beta (β), delta (δ), and omega (ω) groups [28]. In the optimization process, the α, β, and δ agents represent the three best candidate solutions and guide the search dynamics, while the remaining agents constitute the ω group. This hierarchical mechanism enables effective balance between exploration and exploitation.

In this study, GWO was employed to address the multi-peak power characteristics that arise in PV systems under PSC. Its global search capability allows the algorithm to identify the Global Maximum Power Point (GMPP) while reducing steady-state oscillations and avoiding convergence to local maxima. The duty cycle is updated based on the iterative position adjustment of the leading agents, resulting in improved tracking accuracy and faster convergence under changing irradiance.

The encircling behavior of the prey is mathematically described as:

$$D = |C . X_P(t) - X(t)| \quad (12)$$

The position update of the wolves is defined as:

$$X(t+1) = X_p(t) - A \cdot D \quad (13)$$

where:

$$A = 2ar_1 - a \quad (14)$$

$$C = 2r_2 \quad (15)$$

where r_1 and r_2 are random variables uniformly distributed in the range [0,1], and the parameter a decreases linearly from 2 to 0 over the course of iterations. This dynamic adjustment of a governs the balance between exploration (searching new regions of the solution space) and exploitation (refining the current best solutions).

Since the exact location of the global maximum is unknown, the positions of the candidate solutions are updated according to the positions of the three best wolves (α, β, and δ):

$$X(t+1) = \frac{X_\alpha + X_\beta + X_\delta}{3} \quad (16)$$

The objective function corresponds to the instantaneous power delivered by the PV generator:

$$f(V_{PV}, I_{PV}) = P_{PV} = V_{PV} \cdot I_{PV} \quad (17)$$

where V_{PV} and I_{PV} represent the output voltage and current of the PV generator at each iteration.

In this context, each wolf represents a candidate value of the duty cycle applied to the DC-DC converter, while the a solution corresponds to the optimal control command that positions the PV system at its GMPP. Consequently, the GWO-MPPT algorithm dynamically adjusts the converter's duty cycle to maximize the extracted energy, while simultaneously reducing steady-state oscillations and preventing entrapment in local maxima.

B. DTC Control

DTC is considered one of the most significant linear control strategies due to its ease of implementation and fast dynamic response compared to many other control approaches. Relying on this strategy provides significant advantages in terms of performance and efficiency, while simultaneously reducing system complexity and implementation cost. The principle of DTC is based on the direct regulation of the electromagnetic torque and flux of the induction machine. The cornerstone of this method lies in determining the appropriate switching sequence applied to the converter, which is crucial for generating the desired torque and flux levels within the system [29].

The DTC approach depends on the estimation of torque and flux, as these quantities are essential for computing the corresponding torque and flux errors. These errors serve as inputs to the conventional controllers used to regulate both quantities. Within the DTC framework, a Proportional–Integral (PI) regulator is employed to calculate the reference torque based on the speed error. The use of this PI regulator allows the DTC method to achieve closed-loop control of the induction machine, ensuring stable and accurate performance (Figure 4).

The primary objective of DTC is to maintain both the electromagnetic torque and the stator flux amplitude within predefined hysteresis bands by appropriately selecting the inverter's output voltage vector. This is achieved through a real-time decision process which ensures that the machine operates within the desired dynamic performance limits. These characteristics make DTC suitable for PV water pumping applications, where the intermittent nature of solar energy requires fast torque adaptation to power fluctuations to maintain stable motor operation, smooth hydraulic output, and efficient utilization of the available PV power.

The stator flux equations, derived from the induction machine model expressed in a stationary reference frame, are:

$$\begin{cases} \Phi_{s\alpha} = \int_0^t (V_{s\alpha} - R_s \cdot i_{s\alpha}) dt \\ \Phi_{s\beta} = \int_0^t (V_{s\beta} - R_s \cdot i_{s\beta}) dt \end{cases} \quad (18)$$

The stator flux expression is formulated as:

$$\Phi_s = \sqrt{{\Phi_{s\alpha}}^2 + {\Phi_{s\beta}}^2} \quad (19)$$

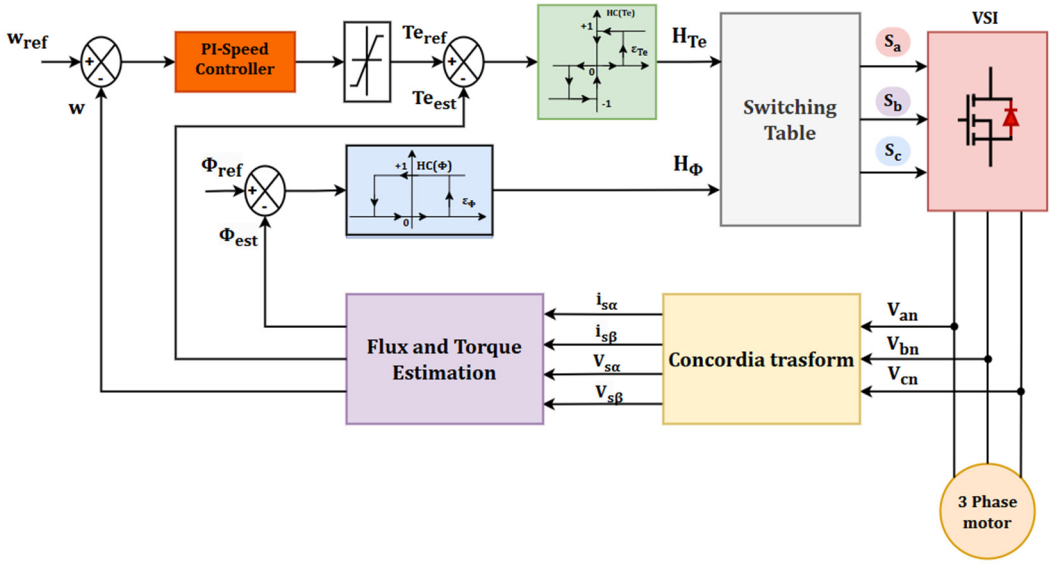

Fig. 4. General implementation of the DTC technique for a three-phase IM.

The electromagnetic torque is then calculated using:

$$T_e = \frac{3 \cdot P}{2}\left[\Phi_{s\alpha} \cdot i_{s\beta} - \Phi_{s\beta} \cdot i_{s\alpha}\right] \quad (20)$$

The estimated flux and torque are compared with their respective reference values, and the resulting errors are fed into two-level Hysteresis Controllers (HC), one dedicated to flux regulation and the other to torque control. These controllers maintain the torque and flux errors within their predefined hysteresis bands, as illustrated in Figure 5. Whenever the torque or flux amplitude approaches the upper or lower limits of the hysteresis comparators, the system selects an appropriate voltage vector to bring the variable back within the specified range of the HC [30]. For flux control:

$$\begin{cases} H_\Phi = 1, \text{if } \varepsilon_\Phi > +HB_\Phi \\ H_\Phi = 0, \text{if } \varepsilon_\Phi < +HB_\Phi \end{cases} \quad (21)$$

where 2HB represents the total width of the hysteresis band of the flux controller.

The torque error ε_{Te} is determined by comparing the estimated torque $\widehat{T_e}$ with its reference value $T_{e_{ref}}$. This error is then applied to a three-level HC, which generates a three-state output variable ($HC_{Te} = -1,0,1$) indicating the desired direction of variation of the electromagnetic torque over time:

$$\begin{cases} H_{Te} = 1, \text{if } \varepsilon_{Te} > +HB_{Te} \\ H_{Te} = -1, \text{if } \varepsilon_{Te} < +HB_{Te} \\ H_{Te} = 0, \text{if } -HB_{Te} < \varepsilon_{Te} < +HB_{Te} \end{cases} \quad (22)$$

TABLE IV. SWITCHING TABLE FOR THE DTC TECHNIQUE

H_Φ	H_{Te}	Sector 1	Sector 2	Sector 3	Sector 4	Sector 5	Sector 6
1	1	V_2	V_3	V_4	V_5	V_6	V_1
1	0	V_0	V_7	V_0	V_7	V_0	V_7
1	-1	V_6	V_1	V_2	V_3	V_4	V_5
0	1	V_3	V_4	V_5	V_6	V_1	V_2
0	0	V_7	V_0	V_7	V_0	V_7	V_0
0	-1	V_5	V_6	V_1	V_2	V_3	V_4

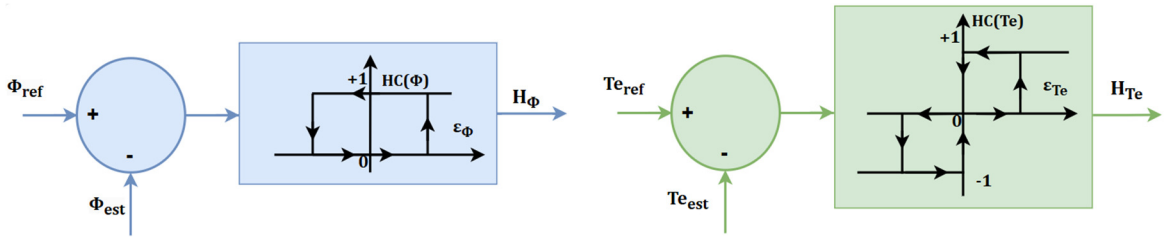

Fig. 5. General diagram of the HC.

C. Methodology and Simulation Setup

The primary objective is to assess the overall system performance under two operating conditions: normal solar irradiance and abnormal conditions resulting from partial shading. For each scenario, two MPPT algorithms are integrated into the DC-DC boost converter, specifically the INC algorithm and the GWO, to ensure optimal tracking of the PV generator's maximum power point.

The adopted approach involves modeling the entire system, including the PV array, DC-DC converter, three-phase inverter, and IM, followed by the implementation of the DTC control strategy, which enables fast and precise regulation of both torque and flux. The performance obtained under the two irradiance conditions is analyzed and compared for both MPPT techniques in terms of energy efficiency, tracking speed, torque and flux stability, and overall pumping efficiency. This comparative assessment makes it possible to identify the most robust and high-performance DTC–MPPT configuration under varying solar irradiance conditions.

1) PV System Structure under Normal Conditions

The structure of the PV system analyzed under normal irradiance conditions consists of a PV generator composed of a single string of modules connected in series. Each string includes six identical PV panels, each rated at 320 W under STC. Consequently, the total power delivered by the generator is approximately 1.92 kW, corresponding to the sum of the individual module power ratings. Under these normal conditions, the PV array provides a total output voltage of 231.6 V and a nominal current of 8.3 A. These values result from the series connection of the module voltages, while the current remains equal to that of a single panel. Table V summarizes the technical characteristics of an individual PV module under standard conditions (irradiance of 1000 W/m² and cell temperature of 25 °C), which serve as the basis for the modeling and simulation of the PV system in this normal operating scenario.

TABLE V. PV PANEL CHARACTERISTICS UNDER STC

Characteristics	Value
Nominal power P_{max}	320 W
Voltage at maximum power point V_{mpp}	38.6 V
Current at maximum power point I_{mpp}	8.3 A
Open-circuit voltage V_{oc}	46.7 V
Short-circuit current I_{sc}	8.76 A
Number of cells	72

The PV panels are connected to the inverter through a boost converter, which adapts the PV generator voltage to the required DC bus level at the inverter input. This converter is controlled by an MPPT unit responsible for real-time optimization of the PV array's operating point. Two optimization strategies are considered in this study: the first is based on the GWO algorithm, while the second employs the INC algorithm. The implementation parameters of both MPPT strategies were selected to ensure stable converter operation and fair performance comparison in both scenarios. For the INC method, the initial duty cycle was set to $D_{init} = 0.3$, while the duty cycle was constrained within the limits $D_{min} = 0.2$and

$D_{max} = 0.45$ to guarantee safe operation of the DC-DC boost converter. A small duty-cycle perturbation of $\Delta D = 2 \times 10^{-5}$ was adopted to minimize steady-state oscillations around the maximum power point, and the switching frequency of the converter was fixed at 10 kHz. For the GWO-based MPPT, a population size of six search agents was selected to balance convergence speed and computational complexity, while the maximum number of iterations was limited to 30 to ensure fast convergence toward the GMPP under variable irradiance conditions. Additional internal variables were employed to manage the exploration-exploitation process, preserve algorithm memory, and regulate duty-cycle updates during the optimization procedure. The conditioned system was then interfaced with a three-phase inverter governed by the DTC method, enabling direct control of the torque and flux of the IM driving the centrifugal pump, as displayed in Figure 6. This electromechanical coupling ensures efficient conversion of solar energy into hydraulic energy, while maintaining optimal performance of the solar pumping system under normal irradiance conditions.

2) *PV System Structure under PSC*

The structure of the PV system analyzed under PSC differs slightly from the normal case in order to reproduce the effects of irradiance variations on the performance of the SWP system. The setup consists of 9 interconnected solar panels, with every three panels subjected to a different level of irradiation (1000 W/m^2, 600 W/m^2 and 200 W/m^2) to simulate the presence of partial shading on part of the PV generator. This configuration enables the analysis of the system's dynamic behavior and the effectiveness of MPPT algorithms when non-uniform illumination occurs. The total peak power of the system under STC is 2.8 kW. Apart from the irradiance distribution, the rest of the system structure remains identical to the previous configuration, including the boost converter, the MPPT block (operating under both GWO and INC approaches), and the three-phase inverter controlled by DTC, which drives the IM coupled to the centrifugal pump, as portrayed in Figure 7.

IV. RESULTS AND DISCUSSION

The P-V curve, shown in Figure 8, exhibits three distinct power peaks, indicating the presence of partial shading on the PV array. The first peak, located at approximately 114 V / 946 W, corresponds to a Local Maximum Power Point (LMPP), the second peak located at 241 V / 1234 W represents the second GMPP, and the third corresponds to the second LMPP at 378 V/ 648 W. This behavior is typical under PSC, where the activation of bypass diodes in shaded modules creates multiple local maxima on the P-V characteristic. In Figure 9, the output power of the boost converter controlled by the INC algorithm quickly stabilizes around 940 W, which corresponds to an LMPP. This indicates that the INC method becomes trapped under partial shading and fails to reach the global optimum. In contrast, Figure 10 shows that the boost converter output power using the GWO fluctuates during its initial search phase but converges after approximately 2.3 s to the GMPP (≈1230 W), confirming its superior tracking accuracy and robustness against local maxima.

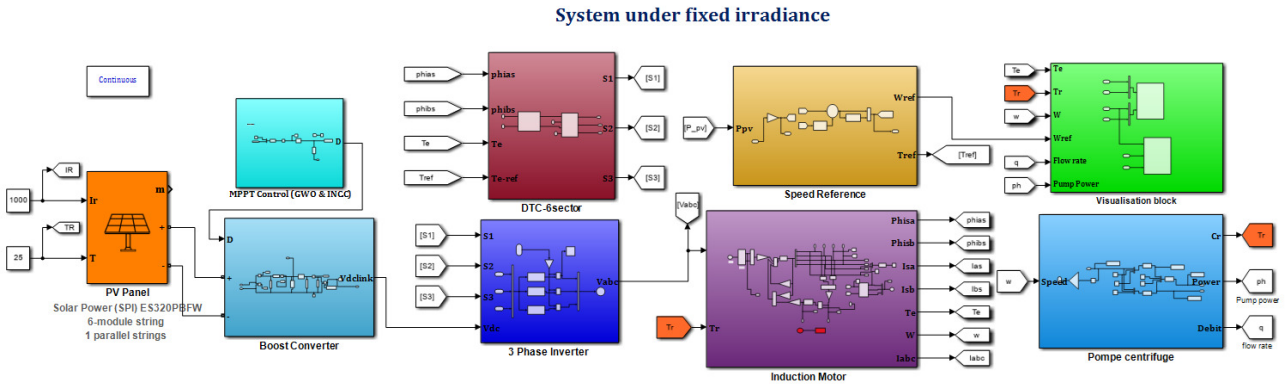

Fig. 6. Simulation of the PV pumping system under normal operating conditions.

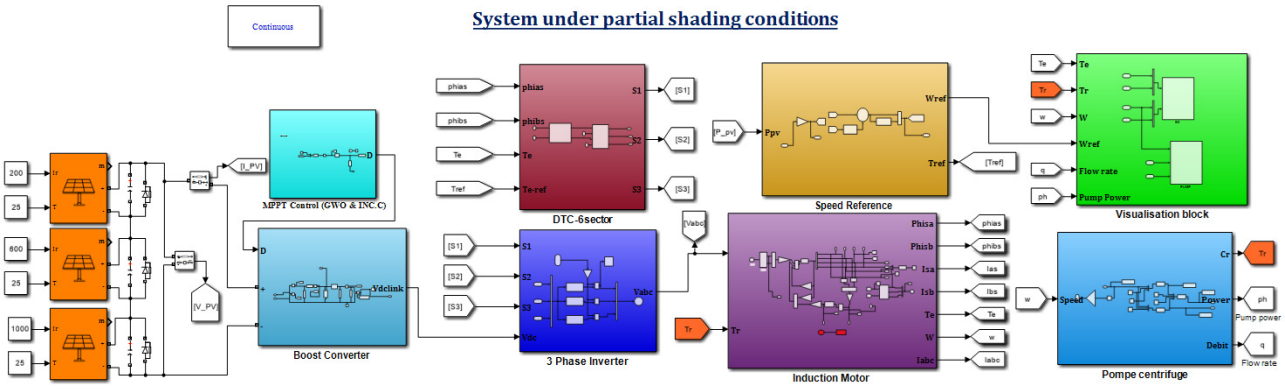

Fig. 7. Simulation of the PV pumping system under partial shading operating conditions.

MATLAB/Simulink simulations were conducted to evaluate the system's dynamic and steady-state behavior under different irradiance scenarios. The comparative analysis between the INC and GWO algorithms focuses on energy efficiency, response dynamics, and system stability. The results demonstrated that the proposed DTC-GWO approach significantly enhances maximum power extraction and operational robustness, particularly under fluctuating solar irradiance conditions.

A. Study under Normal Conditions

1) Normal Pperating Mode (DTC and GWO)

The simulation results indicated that the IM speed reaches its steady-state value of approximately 150 rad/s after a transient period of around 2 s, with no significant overshoot. The electromagnetic torque (T_e) exhibits initial oscillations caused by the GWO optimization process, before stabilizing around 10 N.m, which matches the load torque (T_r). This behavior reflects the establishment of mechanical equilibrium between the motor and the centrifugal pump, as illustrated in Figure 11.

The hydraulic power curve of the pump, exhibited in Figure 12, reaches a steady-state value of approximately 1.5 kW, while the stabilized flow rate is around $5 * 10^{-4}$ m³/s. These results confirm an efficient energy conversion from the PV field to the hydraulic load. The transient variations observed during startup (particularly in torque and power) are attributed to the exploration phase of the GWO, during which the algorithm iteratively searches for the operating point corresponding to the MPP.

Overall, under uniform irradiance conditions, the DTC-GWO combination ensures stable operation, fast MPP tracking, and high system efficiency. The torque stability and accurate speed regulation demonstrate the robustness of the DTC control, while the GWO algorithm provides effective adaptation of the PV power to the motor's demand. These results establish a baseline for comparison with the partial shading scenario, where the performance of the GWO under non-uniform irradiance will be further analyzed.

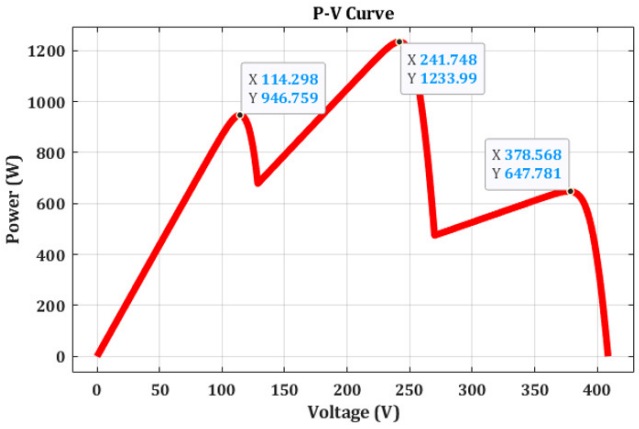

Fig. 8. P-V curve for PV system under PSC.

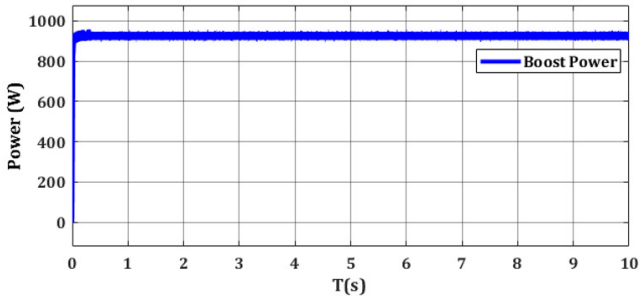

Fig. 9. Boost converter output power using the INC algorithm under PSC.

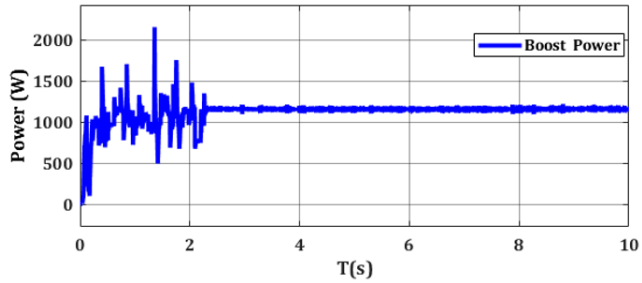

Fig. 10. Boost converter output power using the GWO algorithm under PSC.

2) Normal Operating Mode (DTC and INC)

The IM speed quickly reaches its reference value of 143 rad/s after a rise time of approximately 1.2 s, with a slight oscillation. This response demonstrates the excellent stability of the DTC scheme and the fast dynamic performance of the INC algorithm. The electromagnetic torque (T_e) exhibits an initial peak of 18 N.m during the motor's acceleration phase before stabilizing at 9.2 N.m, matching the load torque (T_r) of the pump. This indicates that mechanical equilibrium between the motor and the hydraulic load is achieved rapidly and in a stable manner (Figure 13).

The hydraulic variables, displayed in Figure 14, follow a similar trend: the pump power settles at approximately 1.3 kW, while the volumetric flow rate stabilizes at $4.8 * 10^{-4}$ m³/s. These results demonstrate that this approach extracts less power than the DTC-GWO, especially in terms of pump power. However, despite its smoother and faster transient response compared to GWO, the INC algorithm remains sensitive to rapid irradiance fluctuations and may face limitations under partial shading scenarios. Therefore, the comparative evaluation with the DTC-GWO configuration under non-uniform conditions is significant to assess the robustness of each approach when subjected to solar energy variations.

B. Study under PSC

1) Partial Shading Mode (DTC and GWO)

In this configuration, the PV generator is subjected to partial shading, represented by 9 series of panels, with every three panels exposed to different irradiance levels. This scenario aims to evaluate the dynamic behavior of the SWP system and the ability of the control strategy to maintain stable operation under non-uniform energy conditions. The model

was simulated in MATLAB/Simulink, employing DTC for IM control and the GWO algorithm for MPPT tracking.

The simulation results, illustrated in Figure 15, show that the electromagnetic torque exhibits significant oscillations during startup, ranging between –2 N.m and +19 N.m, which are attributed to the exploratory behavior of the GWO in its search for the GMPP. After approximately 2.5 s, the torque stabilizes around 7.7 N.m, matching the load torque of the pump, thereby indicating the achievement of mechanical balance between the motor and the hydraulic load.

The IM speed increases gradually before stabilizing around 131 rad/s, with a smooth transition and no noticeable overshoot. The hydraulic parameters exhibit a similar trend: the volumetric flow rate reaches a steady value of approximately $4.4 * 10^{-4}$ m³/s, while the pump power stabilizes at around 1016 W after the transient phase (Figure 16).

These results reveal the capability of the GWO algorithm to effectively track the GMPP in a partially shaded environment, characterized by multiple local maxima. The DTC control ensures the electromechanical stability of the system, maintaining constant torque and speed once the MPP is achieved. The system demonstrates stable, robust, and energy-efficient performance, despite the increased complexity caused by irradiance variations.

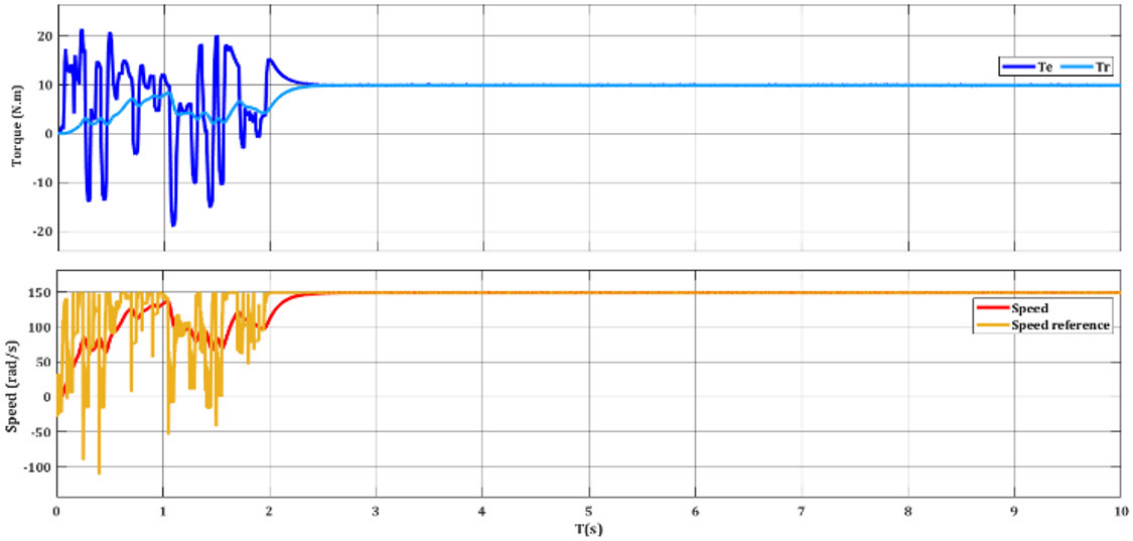

Fig. 11. Response of electromagnetic torque, load torque, and IM speed under normal irradiance conditions using the DTC-GWO strategy.

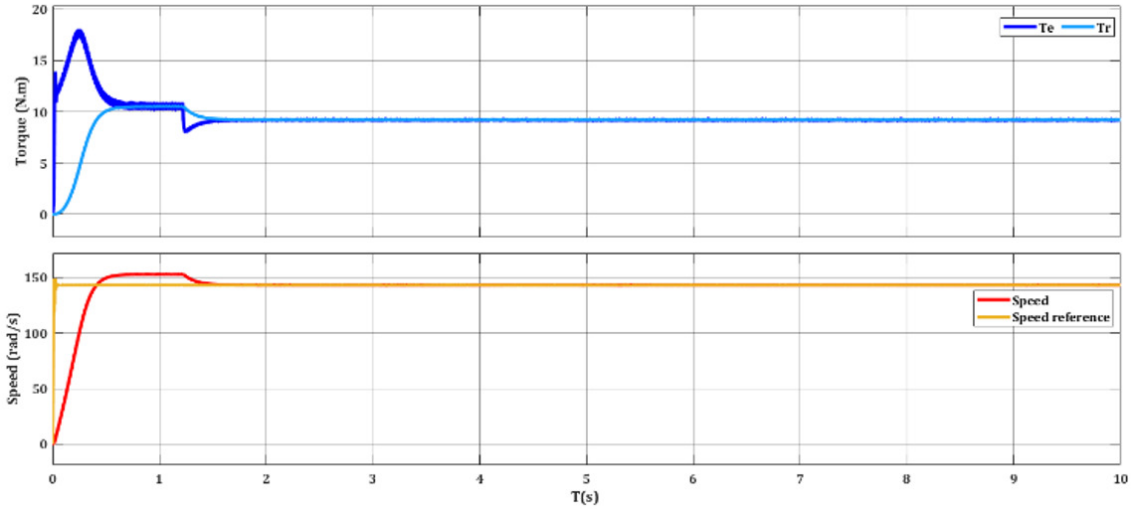

Fig. 12. Speed, flow rate, and pump power curves under normal irradiance conditions using the DTC-GWO strategy.

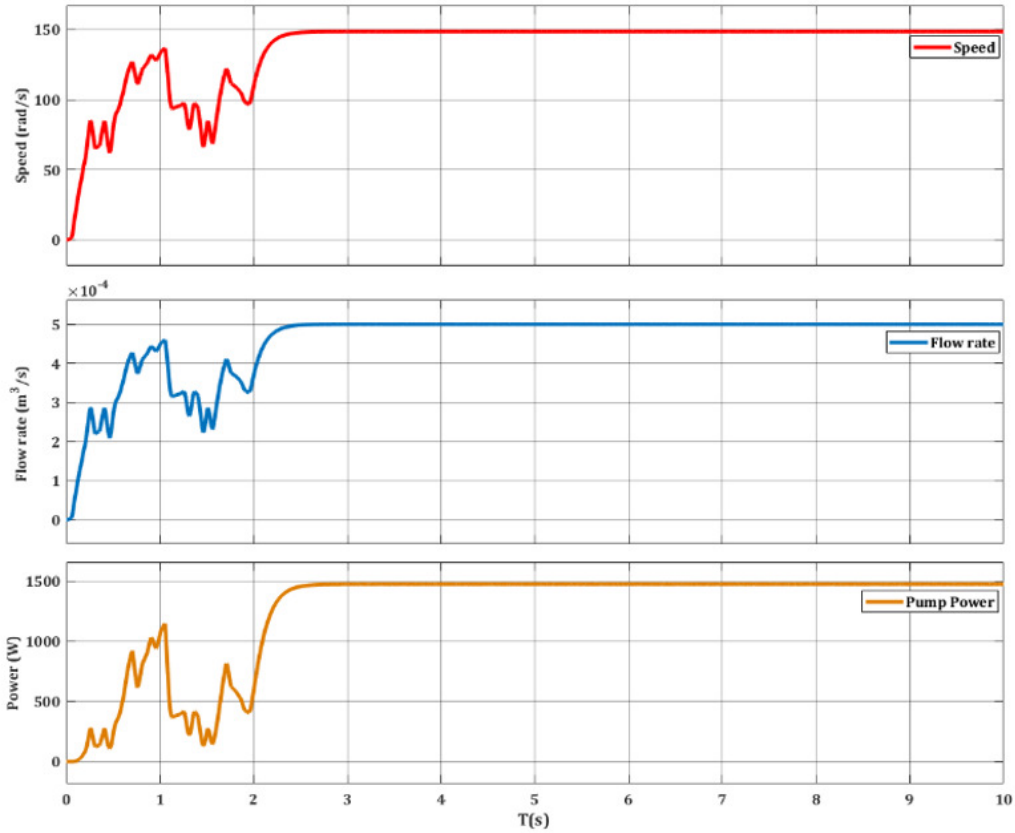

Fig. 13. Response of electromagnetic torque, load torque, and IM speed under normal irradiance conditions using the DTC-INC strategy.

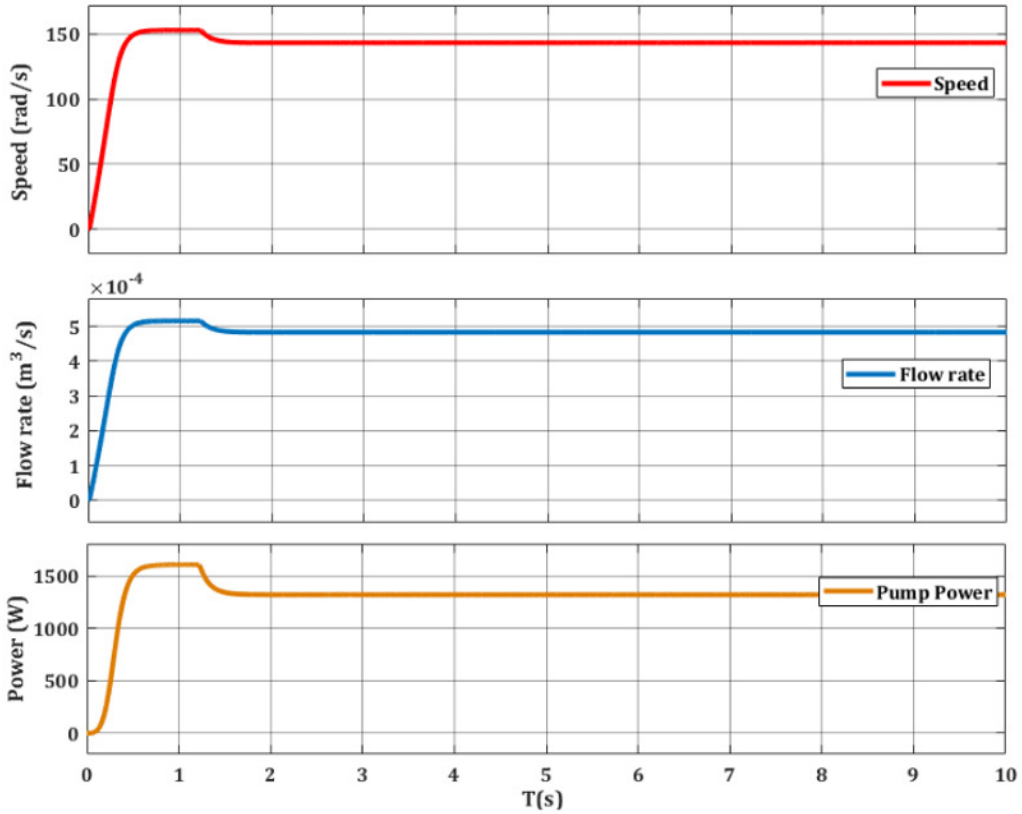

Fig. 14. Speed, flow rate, and pump power curves under normal irradiance conditions using the DTC-INC strategy.

2) Partial Shading Mode (DTC and INC)

Under PSC, with DTC control and INC-based MPPT, the simulation results, shown in Figures 17 and 18, demonstrate a fast and smooth convergence. The electromagnetic torque exhibits an initial peak of approximately 18 N.m, followed by an exponential decrease that stabilizes around 6.4 N.m, matching the T_r. The motor speed reaches 120 rad/s after a rise time of about 0.6 s, with no significant overshoot. The hydraulic variables settle accordingly at the steady-state operating point, with a stabilized flow rate of approximately $4 * 10^{-4}$ m³/s and a hydraulic power output of around 770 W. These results confirm the dynamic stability of the DTC-INC strategy under non-uniform irradiance, with a likely lock-in to a local MPP, which limits operation to low torque and moderate speed, while maintaining steady performance without persistent oscillations. The results obtained under PSC reveal that the fast convergence of the MPPT algorithm does not necessarily correspond to optimal system operation. Although the INC method achieves rapid stabilization, it converges toward an LMPP, resulting in reduced electromagnetic torque and limited hydraulic output power. In contrast, the GWO-based MPPT exhibits transient oscillations during its exploration phase but ultimately identifies the GMPP, leading to higher steady-state torque, speed, and hydraulic power.

These observations indicate that, in PV water pumping applications, robustness to non-uniform irradiance and global optimality are more critical than short-term convergence speed, particularly when the objective is to maximize useful hydraulic energy rather than electrical power alone.

C. Comparison of the Results

The comparative analysis of the obtained results reveals distinct behaviors depending on the operating scenario and the MPPT strategy implemented. Under normal irradiance conditions, both DTC-GWO and DTC-INC configurations exhibit similar steady-state performance in terms of electromagnetic torque, rotational speed, flow rate, and hydraulic power. However, the INC algorithm achieves slightly lower torque (9.2 N.m versus 10 N.m) and speed (143 rad/s versus 150 rad/s), resulting in a reduced hydraulic power of approximately 1320 W compared to 1500 W for the GWO-based control. Despite this, the INC method demonstrates a faster dynamic response, reaching steady state in about 1.2 s, while the GWO controller settles around 2 s. This indicates that, under stable and uniform conditions, the INC method ensures rapid convergence and smooth tracking of the maximum power point, whereas the GWO-based MPPT, although slightly slower, maintains high stability and comparable energy conversion efficiency.

In contrast, under PSC, the difference between the two strategies becomes more pronounced. The GWO-based approach, due to its heuristic and global search capability, successfully identifies the GMPP and maintains a higher energy yield, delivering a torque of 7.7 N.m, a speed of 131 rad/s, a flow rate of $4.4 * 10^{-4}$ m³/s, and a hydraulic power of approximately 1016 W. However, the INC-based configuration, while exhibiting a faster transient, tends to converge prematurely toward a local MPP, leading to a lower operating torque of 6.4 N.m, a speed of 120 rad/s, and an output power of 770 W. These results demonstrate the superior adaptability and robustness of the GWO algorithm in handling non-uniform irradiance conditions, effectively avoiding local optima and maximizing energy capture. In particular, the proposed GWO-based approach achieves an increase of approximately 32% in the delivered hydraulic power compared to the INC method. Conversely, under uniform irradiation conditions, the INC method remains advantageous due to its simplicity, fast convergence, and stable operation.

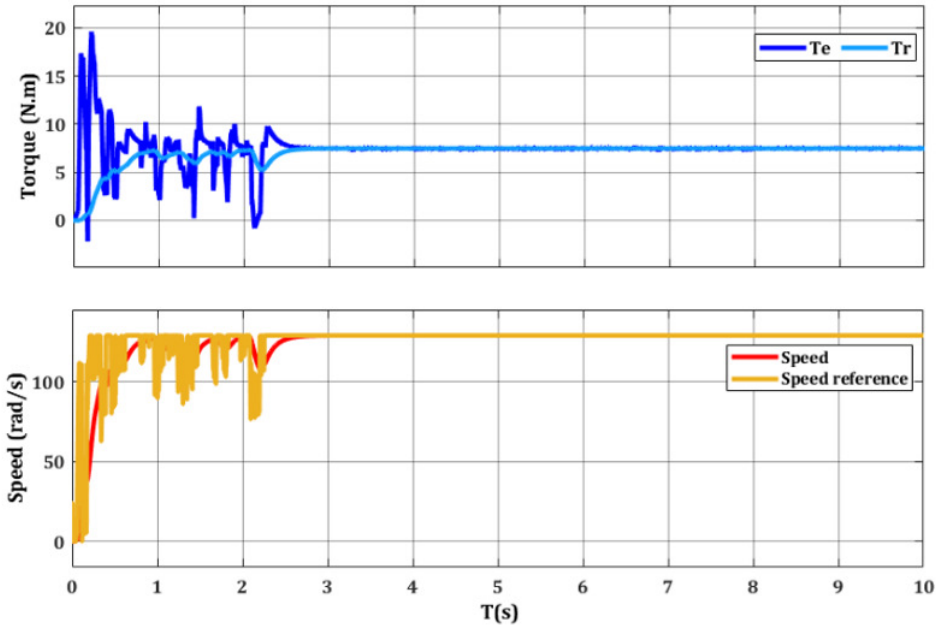

Fig. 15. Response of electromagnetic torque, load torque, and IM speed under PSC using the DTC-GWO strategy.

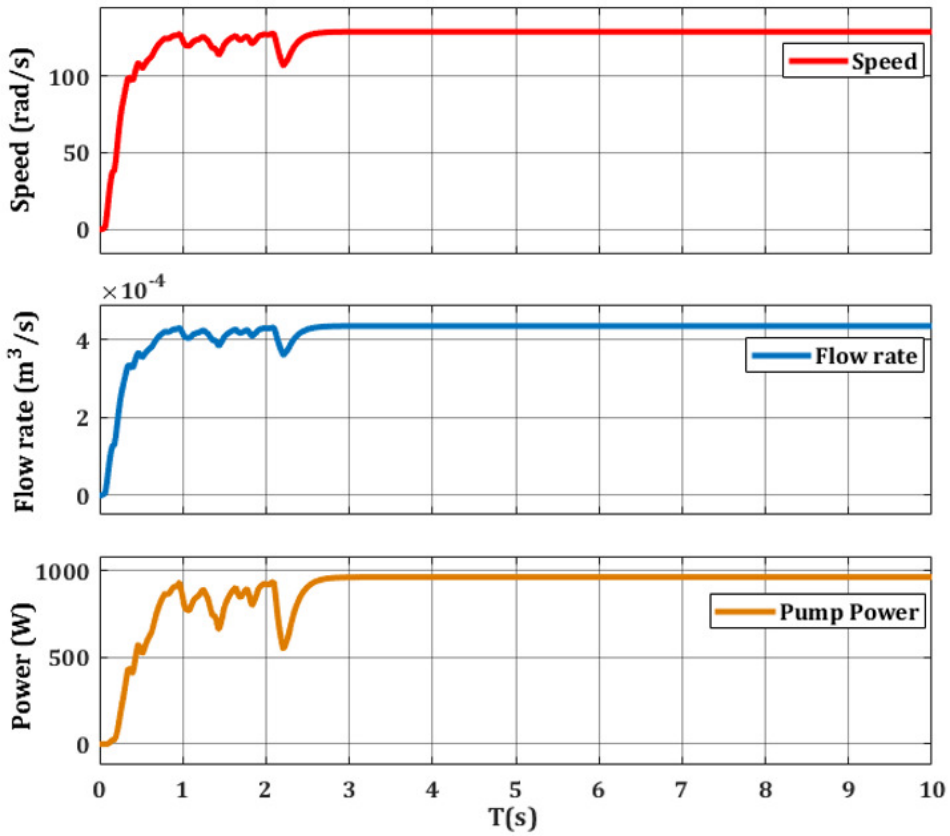

Fig. 16. Speed, flow rate, and pump power curves under PSC using the DTC-GWO strategy.

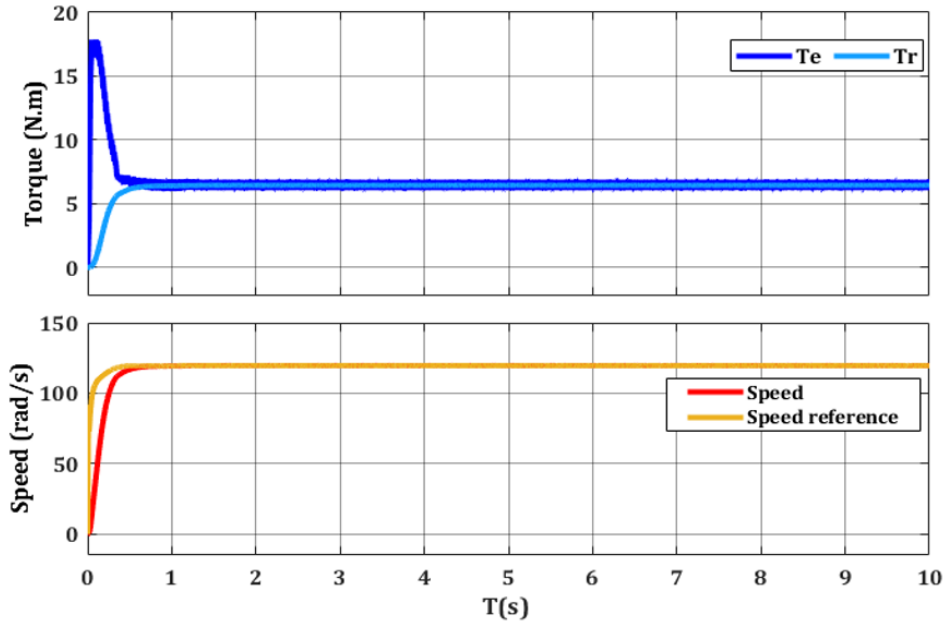

Fig. 17. Response of electromagnetic torque, load torque, and IM speed under PSC using the DTC-INC strategy.

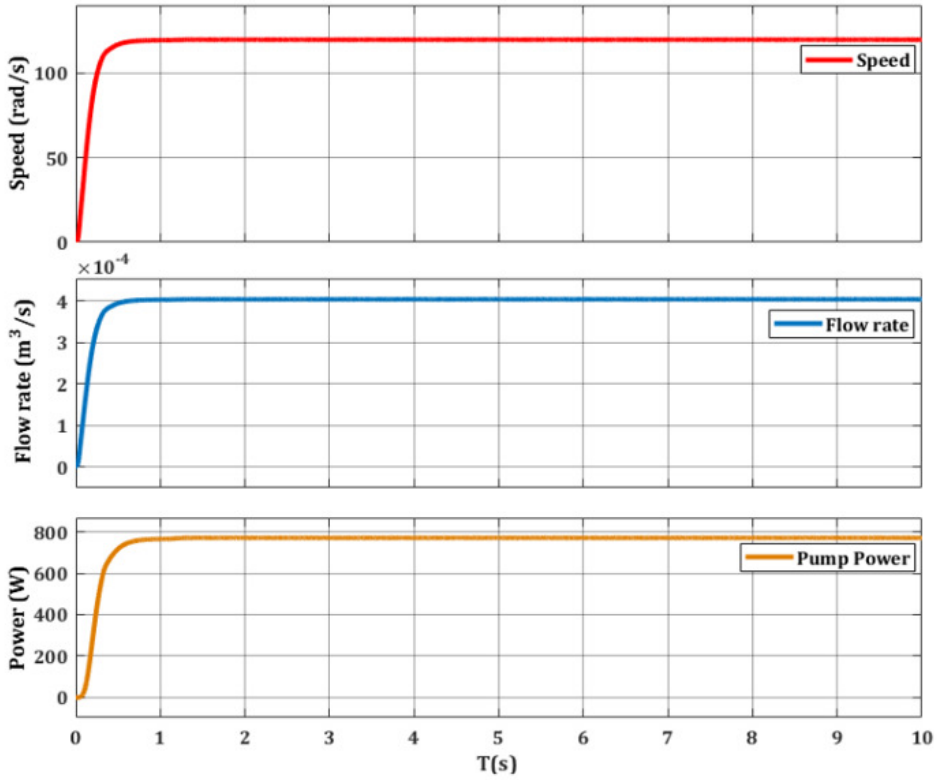

Fig. 18. Speed, flow rate, and pump power curves under PSC using the DTC-INC strategy.

TABLE VI. COMPARISON OF SWP SYSTEM PERFORMANCE UNDER DIFFERENT IRRADIANCE CONDITIONS FOR TWO MPPT STRATEGIES (DTC-GWO AND DTC-INC).

Scenario	MPPT	Couple (Te) [N.m]	Speed (w) [rad/s]	Flow rate (Q) [$\times 10^{-4}$ m^3/s]	Pump power [W]	Settling time
Normal	GWO	10	150	5	1500	≈ 2 s
Normal	INC	9.2	143	4.8	1320	≈ 1.2 s
Partial shading	GWO	7.7	131	4.4	1016	≈ 2.5s
Partial shading	INC	6.4	120	4	770	≈ 0.6 s

V. CONCLUSIONS

This study effectively carried out a performance analysis of a Photovoltaic (PV) water pumping system driven by an Induction Motor (IM) controlled through Direct Torque Control (DTC) and integrated with two Maximum Power Point Tracking (MPPT) techniques: the Incremental Conductance (INC) algorithm and the Grey Wolf Optimizer (GWO). The obtained simulation results demonstrated that, under uniform irradiance conditions, both control strategies achieved comparable performance in terms of electromagnetic torque, rotational speed, flow rate, and hydraulic power output. The DTC-INC configuration exhibited a faster response and smoother dynamic behavior. Under Partial Shading Conditions (PSC), however, the difference between the two approaches became more significant. The GWO-based MPPT, due to its adaptive and heuristic exploration capability, successfully located the Global Maximum Power Point (GMPP) and ensured higher hydraulic efficiency and enhanced energy extraction from the PV generator, resulting in an improvement of approximately 32% in hydraulic power compared to the INC algorithm. Conversely, the INC algorithm, despite its faster convergence, tended to lock onto a local maximum, thereby limiting the overall performance. Consequently, the DTC-GWO approach demonstrated superior robustness, stability, and power extraction capability under non-uniform irradiance.

Future work will focus on developing a hybrid MPPT strategy that combines the rapid convergence of INC with the global search capability of GWO, enabling fast, accurate, and stable power point tracking under variable irradiance. Further investigations will include experimental validation, energy storage integration to mitigate power fluctuations, and the extension of the proposed strategy to other motor types, such as Permanent Magnet Synchronous Machines (PMSMs), to broaden its application in intelligent Solar Water Pumping (SWP) systems.

ACKNOWLEDGMENT

This work is supported by the Green Energy Park research platform, Morocco (Mohamed VI Polytechnic University, Benguerir / Research Institute in Solar Energy and New Energies, IRESEN).

REFERENCES

[1] "Renewable capacity statistics 2024," International Renewable Energy Agency (IRENA). https://www.irena.org/Publications/2024/Mar/Renewable-capacity-statistics-2024.

[2] E. H. Ibrahim and S. R. Aslan, "Solar photovoltaic water pumping system approach for electricity generation and irrigation: Review," *Diagnostyka*, vol. 24, no. 2, pp. 1–7, 2023, https://doi.org/10.29354/diag/165849.

[3] T. Mahoney, "Insights from GOGLA's 2024 Sales and Impact Data." GOGLA. https://gogla.org/reports/semi-annual-solar-market-report/insights-from-goglas-2024-sales-and-impact-data/.

[4] "Spotlight on Solar Water Pumps." CLASP. https://www.clasp.ngo/report/net-zero-heroes/spotlights/spotlight-on-solar-water-pumps/.

[5] O. Idbouhouch, N. Rabbah, N. Lamrini, H. Oufettoul, I. A. Abdelmoula, and M. Zegrari, "Assessing PV inverter efficiency degradation under semi-arid conditions: A case study in Morocco," *Heliyon*, vol. 10, no. 17, Sept. 2024, https://doi.org/10.1016/j.heliyon.2024.e36906.

[6] M. A. Elgendy, B. Zahawi, and D. J. Atkinson, "Assessment of Perturb and Observe MPPT Algorithm Implementation Techniques for PV Pumping Applications," *IEEE Transactions on Sustainable Energy*, vol. 3, no. 1, pp. 21–33, Jan. 2012, https://doi.org/10.1109/TSTE.2011.2168245.

[7] A. Elgharbi, D. Mezghani, and A. Mami, "Intelligent Control of a Photovoltaic Pumping System," *Engineering, Technology & Applied Science Research*, vol. 9, no. 5, pp. 4689–4694, Oct. 2019, https://doi.org/10.48084/etasr.2982.

[8] A. A. A. El-Hassan, G. E.-S. A. Taha, A. M. Yousef, and E.-N. A. Ibrahim, "Analysis and control of grid connected PV system under partial shading," in *24th International Middle East Power System Conference* (*MEPCON*), Egypt, Dec. 19–21, 2023, pp. 1–7, https://doi.org/10.1109/MEPCON58725.2023.10462451.

[9] J. Ahmed and Z. Salam, "A critical evaluation on maximum power point tracking methods for partial shading in PV systems," *Renewable and Sustainable Energy Reviews*, vol. 47, pp. 933–953, July 2015, https://doi.org/10.1016/j.rser.2015.03.080.

[10] M. M. Shehu, M. Dong, and J. Hu, "Optimization of Particle Swarm based MPPT under Partial Shading Conditions in Photovoltaic Systems," in *16th IEEE Conference on Industrial Electronics and Applications* (*ICIEA*), Chengdu, China, Aug.. 1–4, 2021, pp. 267–272, https://doi.org/10.1109/ICIEA51954.2021.9516360.

[11] K. Xia, Y. Li, and B. Zhu, "Improved Photovoltaic MPPT Algorithm Based on Ant Colony Optimization and Fuzzy Logic Under Conditions of Partial Shading," *IEEE Access*, vol. 12, pp. 44817–44825, March 2024, https://doi.org/10.1109/ACCESS.2024.3381345.

[12] S. Mohanty, B. Subudhi, and P. K. Ray, "A New MPPT Design Using Grey Wolf Optimization Technique for Photovoltaic System Under Partial Shading Conditions," *IEEE Transactions on Sustainable Energy*, vol. 7, no. 1, pp. 181–188, Jan. 2016, https://doi.org/10.1109/TSTE.2015.2482120.

[13] K. Atici, I. Sefa, and N. Altin, "Grey Wolf Optimization Based MPPT Algorithm for Solar PV System with SEPIC Converter," in *4th International Conference on Power Electronics and their Applications* (*ICPEA*), Elazig, Turkey, Sept. 25–27, 2019, pp. 1–6, https://doi.org/10.1109/ICPEA1.2019.8911159.

[14] O. Id Bouhouch, N. Rabbah, H. Oufettoul, A. Benazzou, I. A. Abdelmoula, and M. Zegrari, "Comparative Analysis of Three-Phase Photovoltaic Inverters Control Techniques," in *Proceedings of the 4th International Conference Smart Applications and Data Analysis* (*SADASC*), Marrakesh, Morocco, Sept. 22–24, 2022, pp. 443–456, https://doi.org/10.1007/978-3-031-20490-6_35.

[15] A. Nouaiti, M. Reddak, C. Boutahiri, A. Mesbahi, A. M. Hsaini, and A. Bouazi, "A Single Stage Photovoltaic Solar Pumping System based on the Three Phase Multilevel Inverter," *Engineering, Technology & Applied Science Research*, vol. 13, no. 6, pp. 12145–12150, Dec. 2023, https://doi.org/10.48084/etasr.6403.

[16] A. G. M. A. Aziz, A. Y. Abdelaziz, Z. M. Ali, and A. A. Z. Diab, :A Comprehensive Examination of Vector-Controlled Induction Motor Drive Techniques," *Energies*, vol. 16, no. 6, 2023, Art. no. 2854, https://doi.org/10.3390/en16062854.

[17] I. Takahashi and T. Noguchi, "A New Quick-Response and High-Efficiency Control Strategy of an Induction Motor," *IEEE Transactions on Industry Applications*, vol. IA-22, no. 5, pp. 820–827, Sept. 1986, https://doi.org/10.1109/TIA.1986.4504799.

[18] M. Depenbrock, "Direct self-control (DSC) of inverter fed induktion machine," in *IEEE Power Electronics Specialists Conference*, Blacksburg, USA, June 21–26, 1987, pp. 632–641, https://doi.org/10.1109/PESC.1987.7077236.

[19] I. Saady, M. Karim, B. Bossoufi, N. El Ouanjli, S. Motahhir, and B. Majout, "Optimization and control of photovoltaic water pumping system using kalman filter based MPPT and multilevel inverter fed DTC-IM," *Results in Engineering*, vol. 17, Mar. 2023, Art. no. 100829, https://doi.org/10.1016/j.rineng.2022.100829.

[20] S. Shukla and B. Singh, "A PV-Grid Fed DTC Based Induction Motor Drive for Water Pumping," in *IEEE Energy Conversion Congress and Exposition* (*ECCE*), Portland, USA, Sept. 23–27, 2018, pp. 3400–3405, https://doi.org/10.1109/ECCE.2018.8557624.

[21] O. Idbouhouch, M. Zegrari, N. Rabbah, I. A. Abdelmoula, H. Oufettoul, and S. Motahhir, "Embedded implementation of phase imbalance faults in three-phase inverters: The impact of MOSFET conduction resistance variations," *Results in Engineering*, vol. 26, June 2025, Art. no. 105227, https://doi.org/10.1016/j.rineng.2025.105227.

[22] M. Chahartaghi and A. Nikzad, "Exergy, environmental, and performance evaluations of a solar water pump system," *Sustainable Energy Technologies and Assessments*, vol. 43, Feb. 2021, Art. no. 100933, https://doi.org/10.1016/j.seta.2020.100933.

[23] C. Mademlis, I. Kioskeridis, and T. Theodoulidis, "Optimization of single-phase induction Motors-part I: maximum energy efficiency control," *IEEE Transactions on Energy Conversion*, vol. 20, no. 1, pp. 187–195, Mar. 2005, https://doi.org/10.1109/TEC.2004.842386.

[24] C. Moulay-Idriss and B. Mohamed, "Application of the DTC control in the photovoltaic pumping system," *Energy Conversion and Management*, vol. 65, pp. 655–662, Jan. 2013, https://doi.org/10.1016/j.enconman.2011.08.026.

[25] M. B. de Rossiter Correa, C. B. Jacobina, A. M. N. Lima, and E. R. C. da Silva, "Rotor-flux-oriented control of a single-phase induction motor drive," *IEEE Transactions on Industrial Electronics*, vol. 47, no. 4, pp. 832–841, Aug. 2000, https://doi.org/10.1109/41.857963.

[26] S. Ziaeinejad, Y. Sangsefidi, H. Pairodin Nabi, and A. Shoulaie, "Direct Torque Control of Two-Phase Induction and Synchronous Motors," *IEEE Transactions on Power Electronics*, vol. 28, no. 8, pp. 4041–4050, Aug. 2013, https://doi.org/10.1109/TPEL.2012.2230409.

[27] S. Abouda, F. Nollet, A. Chaari, N. Essounbouli, and Y. Koubaa, "Direct torque control-DTC of induction motor used for piloting a centrifugal pump supplied by a photovoltaic generator," *International Journal of Electrical, Computer and Communication Engineering*, vol. 7, no. 8, pp. 1110–1115, 2013.

[28] N. Pamuk, "Performance Analysis of Different Optimization Algorithms for MPPT Control Techniques under Complex Partial Shading Conditions in PV Systems," *Energies*, vol. 16, no. 8, 2023, Art. no. 3358, https://doi.org/10.3390/en16083358.

[29] R. Sadouni, M. Sahnoun, I. Zababe, and H. Reghioui, "Direct Torque Control of Dual Three Phase Induction Motor fed by Direct Power Control Rectifier using Fuzzy Logic Speed Controller," *Science, Engineering and Technology*, vol. 5, no. 1, pp. 154–162, Jan. 2025, https://doi.org/10.54327/set2025/v5.i1.173.

[30] S. Krim, S. Gdaim, A. Mtibaa, and M. F. Mimouni, "FPGA contribution in photovoltaic pumping systems: models of MPPT and DTC-SVM algorithms," *International Journal of Renewable Energy Research*, vol. 6, no. 3, pp. 866–879, 2016.